Symmetry breaking and localization in quantum chaotic systems

M. Thaha and R. Blümel
Department of Physics, University of Delaware, Newark, Delaware 19716

U. Smilansky
Department of Physics, The Weizmann Institute, 76100 Rehovot, Israel
(Received 16 April 1993)

Breaking an antiunitary symmetry modifies the localization length. In analogy to results obtained recently in the context of Anderson localization in disordered solids, we establish that the localization length λ of dynamically localizing quantum chaotic systems depends on the invariance properties of the system under antiunitary symmetry operations. We consider a Hamiltonian system—a modified version of the kicked rotor—which, by tuning its parameters, can change its invariance properties in a manner similar to the (Gaussian orthogonal ensemble)→(Gaussian unitary ensemble)→(Gaussian symplectic ensemble) transitions ($\beta = 1 \to \beta = 2 \to \beta = 4$) in Dyson's theory of random matrices. We find that λ depends on the universality class according to $\lambda(\beta) = \beta\lambda(\beta = 1)$. This relation holds as long as the corresponding classical diffusion constant is kept at a fixed value. Based on semiclassical arguments substantiated by an extensive numerical study of the symplectic kicked rotor, we show that the transition between different universality classes is a smooth function of the symmetry-breaking interaction. For the transition from the orthogonal to the unitary class ($\beta = 1 \to \beta = 2$), the semiclassical theory provides an approximate expression for the transition function as well as the critical strength of the symmetry-breaking interaction necessary to achieve the full factor-of-2 increase of the localization length. Universal scaling functions describe the crossover between the diffusive regime and the Anderson localized regime for all three universality classes. The three functions are very similar and, within a few percent, can be reproduced by a single function.

PACS number(s): 05.45.+b, 72.15.Rn

I. INTRODUCTION

Antiunitary symmetries play an important role in the description and classification of quantum systems. Unlike unitary symmetries, they do not lead to conserved quantum numbers. But the presence or absence of an antiunitary symmetry can have profound and measurable consequences for the observables of a quantum system. The effect is universal. This means that breaking an antiunitary symmetry results in a multiplication of the magnitudes of system observables by universal factors whose precise numerical values depend on the presence (or absence) of additional unitary or antiunitary symmetries. Well-known examples are cross sections, transition probabilities, spectral statistics, and resonance widths [1]. In case an antiunitary symmetry is based on a classical invariance (for instance, time reversal invariance) the effect of breaking this symmetry is much less pronounced—if not entirely absent—on the classical level. Thus the importance of antiunitary symmetries is a feature of quantum systems and does not have a classical analog.

Another purely quantum feature without a classical analog is Anderson localization. This phenomenon, first discoverd in the study of electron transport in disordered solids [2], was also found in certain deterministic Hamiltonian systems whose classical counterpart is chaotic. A paradigm example is the quantum kicked rotor [3–8] but localization also occurs in other systems such as periodically perturbed surface state electrons [9,10] or Rydberg atoms in strong microwave fields [11,12]. These rather simple dynamical systems and the disordered (quasi-one-dimensional) solid share three important properties which enable the onset of Anderson localization: (i) the classical phase space is extended, (ii) diffusion characterizes the classical evolution of trajectory ensembles, and (iii) many trajectories contribute to the same transition and the corresponding quantum amplitudes are endowed with phases which are sufficiently uncorrelated to induce Anderson localization as a result of intricate interferences.

Breaking an antiunitary symmetry modifies the localization length. For disordered systems this effect was predicted by several authors [13,14]. They obtained the result

$$\lambda(\beta) = \beta\lambda(\beta = 1) \quad . \tag{1.1}$$

Here, λ is the localization length and $\beta = 1, 2, 4$ is the Dyson parameter characterizing the universality class of the system involved: $\beta = 1$ (4) for time reversal invariant disordered systems which do not (or do) involve spin degrees of freedom and $\beta = 2$ for systems with broken time reversal symmetry.

The relation (1.1) makes sense only if the symmetry-breaking interaction does not change the diffusion properties of the underlying classical system. Therefore, in devising experiments and theoretical models to study the

effect (1.1), great care has to be taken to ensure this condition. We emphasize that in a typical nonlinear system this is an elusive goal. Even small changes in the symmetry-breaking interaction can change phase-space structures dramatically with an accompanying drastic effect on the classical diffusion constant D. This statement is strictly true in case there is only one parameter controlling the symmetry-breaking interaction. In case the symmetry-breaking interaction depends on two control parameters, it is possible to study the effect of symmetry-breaking on lines of constant D in the two-dimensional parameter space. But this procedure may take us into phase-space regions which we do not wish to explore. Also it limits the way in which the symmetry is broken to a one-dimensional subspace of the full parameter space. Therefore, in the one-parameter case, or if we do not want to impose any restrictions in the two-parameter case (or N-parameter case, in general) the best we can do is to keep the diffusion properties of the system constant on average. The residual oscillations in the diffusion constant can be taken into account by normalizing the localization length to the classical diffusion constant D. Our model system, to be discussed in Sec. II, is defined in this spirit.

The prediction (1.1) was checked experimentally in magneto-transport measurements [14]. The case $\beta = 2$ was realized with the help of a Si-doped GaAs sample. In this material the spin effects are small. Breaking time reversal by switching on a magnetic field should result in a doubling of the localization length according to (1.1). This was indeed observed. In a $Y_{0.3}Si_{0.7}$ sample in which spin-orbit scattering is large, a transition from $\beta = 4$ to $\beta = 2$ was observed when switching on a magnetic field. The accompanying halving of the localization length was observed [14].

In the present paper we study the effects of an antiunitary symmetry on the localization length of quantum chaotic systems and compare them with the known results for disordered solids. Contrary to disordered solids, localization in quantum chaotic systems is not brought about by externally introduced randomness but is self-induced by the underlying chaotic classical dynamics. Therefore an intriguing question of central importance is whether (1.1) derived in the context of disordered solids holds in the context of dynamically localizing systems with a chaotic classical limit. Based on semiclassical arguments supported by extensive numerical tests we show that this is indeed the case. Moreover, we show that the localization length is a continuous function of the symmetry-breaking interaction and a universal function describes the transition between the diffusive regime and the Anderson localized regime.

In order to illustrate our results, we study the symplectic kicked rotor recently introduced by Scharf [15]. The symplectic kicked rotor is constructed by coupling a spin-$\frac{1}{2}$ degree of freedom to the standard kicked rotor, which results in

$$H = \tfrac{1}{2}\tau\hat{l}^2 + k\left(V_0(\theta) + \sum_{i=1}^{3} V_i(\theta)\sigma_i\right)\delta_p(t) \ . \quad (1.2)$$

Here, $V_j(\theta)$, $j = 0,\ldots,3$ are 2π periodic functions, $\sigma_1 \equiv \sigma_x$, $\sigma_2 \equiv \sigma_y, \sigma_3 \equiv \sigma_z$ are the Pauli matrices, θ is the rotation angle, $\hat{l}$ is the angular-momentum operator ($\hat{l} = -i\partial/\partial\theta$), and $\delta_p(t)$ is the 1-periodic δ function. τ and k are control parameters. The Hamiltonian (1.2) is powerful enough to exhibit all three statistical universality classes. A certain class is selected by an appropriate choice of potentials V_j. Quantizing the rotor on a torus, Scharf was able to represent the Hamiltonian (1.2) as a matrix of finite dimension. He chose $V_0(\theta) = \cos(\theta)$, $V_i(\theta) = v_i \sin(v_i\theta)$, $i = 1,2,3$, and imposed the boundary condition $\psi(\theta + 2\pi) = \exp(ia)\,\psi(\theta)$ (Bloch condition in the resonance case). For Bloch number $a = \ln 2$, $K = 5$, $\tau = 8\pi/401$, ($k \approx 79.78$), $v_1 = 0.1$, $v_2 = 0.2$, $v_3 = 0.3$, he showed that the nearest-neighbor statistics of the one-cycle propagator of (1.2) exhibits properties of the CUE ensemble, while for Bloch number $a = 0$ CSE properties are obtained. Here and in the following COE, CUE, and CSE will denote the three Dyson ensembles, the circular orthogonal, unitary, and symplectic ensembles [16–18], respectively. These three universality classes are associated with $\beta = 1, 2$, and 4, respectively.

In order to study the localization properties of (1.2) and its behavior when switching between universality classes, we focus on the nonresonant case by quantizing the rotor on a cylinder. This approach yields a nonreducible, infinite-dimensional one-cycle propagator. We will show that in a basis smaller than the localization length, the nonresonant one-cycle operator exhibits COE, CUE, and CSE properties for appropriate choices of parameters in (1.2). This enables us to study the localization length for all three universality classes in a single model system.

As was already emphasized above, the comparison of localization lengths for the different universality classes is meaningful only if the results are properly normalized to the respective classical diffusion constants. For the CUE rotor we were able to derive analytical expressions for the diffusion constant by extending a diagrammatic method [19,20] which was already successfully applied to the standard kicked rotor. The analytical formulas obtained turned out to be in very good overall agreement with numerical Monte Carlo calculations.

For the general CSE rotor it is difficult to define the corresponding classical system which is necessary for calculating the classical diffusion constant. Questions relating to this issue are discussed in Sec. IV. Nevertheless, by studying the mapping of the quantum mechanical energy expectation value in Sec. IV D, we were able to extract a zeroth-order expression for what can be identified with the classical diffusion constant in this case.

The paper is organized as follows. In Sec. II we present our model [constructed from (1.2)] and discuss its symmetries for special limiting choices of the control parameters. We also study the quasienergy statistics of the one-cycle propagator of the model Hamiltonian and present a chart which maps the control parameters of the system onto the corresponding universality classes. In Sec. III we expand considerably on the CUE limit of the symplectic kicked rotor already discussed briefly in Ref. [21]. In Sec. IV we discuss the CSE limit of the symplectic kicked

rotor. We establish that in all three limiting cases, i.e., COE, CUE, and CSE, the staying probability [22] can be derived from a universal scaling function which describes the transition between the diffusive regime and the Anderson localized regime. Calculating the ratio of the participation ratio and the diffusion constant for the symplectic rotor, we establish the validity of (1.1) for the localization length of the symplectic kicked rotor. Section V concludes the paper with a brief summary and discussion of our results.

II. THE MODEL

Throughout this paper we use

$$H = \tfrac{1}{2}\tau\hat{l}^2 + k\left[\cos\left(\frac{\pi p}{2}\right)\cos\left(\frac{\pi q}{2}\right)\cos(\theta) + \tfrac{1}{2}\cos\left(\frac{\pi p}{2}\right)\sin\left(\frac{\pi q}{2}\right)\sin(2\theta)\sigma_x + \sin\left(\frac{\pi p}{2}\right)\sin(\theta)\sigma_z\right]\delta_p(t)\ , \tag{2.1}$$

which is a special case of (1.2). The meaning of the symbols in (2.1) is the same as in (1.2). We introduced the "symmetry-breaking parameters" p and q which allow us to switch between different symmetry classes (see Secs. II C and II D below).

As was discussed already in the Introduction, it is of utmost importance to control the diffusion properties of the Hamiltonian (2.1) for a meaningful comparison of the localization lengths for the different symmetry classes. The form of the Hamiltonian (2.1) was suggested by our desire to keep the diffusion properties of (2.1) constant under a change of the symmetry-breaking parameters p and q. In the case $p = 0$ the diffusion is indeed constant on average. This is shown in detail in Sec. III. In Sec. IV we will show that this also holds for the special cases $q = 0$ and $p = 1$. For the more general case $p \neq 0$, $q \neq 0$ we will show in Sec. IV D that the average diffusion constant is only weakly dependent on p and q.

For some investigations it is advantageous to write (2.1) in the form

$$H = \tfrac{1}{2}\tau\hat{l}^2 + \kappa[\cos(\theta) + \tfrac{1}{2}\mu\sin(2\theta)\sigma_x + \varepsilon\sin(\theta)\sigma_z]\delta_p(t). \tag{2.2}$$

The mapping between the two notations, $(k,p,q) \to (\kappa,\mu,\varepsilon)$ is given by

$$\begin{aligned}\kappa &= k\cos\left(\frac{\pi p}{2}\right)\cos\left(\frac{\pi q}{2}\right)\ ,\\ \mu &= k\cos\left(\frac{\pi p}{2}\right)\sin\left(\frac{\pi q}{2}\right)\Big/\kappa\ ,\\ \varepsilon &= k\sin\left(\frac{\pi p}{2}\right)\Big/\kappa\quad .\end{aligned} \tag{2.3}$$

The inverse mapping, $(\kappa,\mu,\varepsilon) \to (k,p,q)$ is given by

$$k = \kappa\sqrt{1+\mu^2+\varepsilon^2}\ ,\quad p = \frac{2}{\pi}\arctan\left[\frac{\varepsilon}{\sqrt{1+\mu^2}}\right]\ ,\quad q = \frac{2}{\pi}\arctan(\mu)\quad . \tag{2.4}$$

Apart from our desire to make the classical diffusion constant as weakly dependent on the symmetry-breaking parameters as possible, the form of the Hamiltonian (2.1) was chosen such that for special values of the symmetry-breaking parameters (2.1) reduces to variants of the kicked rotor already studied in the literature.

A. Special cases

(i) $p = q = 0$: In this case the Hamiltonian (2.1) describes the standard kicked rotor [3,4,8] whose associated classical dynamics is known as the standard mapping [23]. This Hamiltonian is probably the most widely studied time-dependent Hamiltonian in the literature. It yielded surprising results on localization in quantum dynamic systems [3–5,24] and was used to study the effects of weak localization in the kicked rotor [22].

(ii) $p = 0$, $q \neq 0$: In the representation in which σ_x is diagonal the resulting Hamiltonian is equivalent with the Hamiltonian used in Ref. [21] to study the influence of symmetry breaking in quantum chaotic systems.

(iii) $p \neq 0$, $q = 0$: In this case the Hamiltonian (2.1) reads

$$H = \tfrac{1}{2}\tau\hat{l}^2 + k\left[\cos\left(\frac{\pi p}{2}\right)\cos(\theta) + \sin\left(\frac{\pi p}{2}\right)\sin(\theta)\sigma_z\right]\delta_p(t). \tag{2.5}$$

In the standard representation in which σ_z is diagonal this Hamiltonian is equivalent with two decoupled Hamiltonians $H_\uparrow = \frac{1}{2}\tau\hat{l}^2 + k\cos(\theta - \frac{\pi p}{2})$ and $H_\downarrow = \frac{1}{2}\tau\hat{l}^2 + k\cos(\theta + \frac{\pi p}{2})$. Shifting θ by $\pm\frac{\pi p}{2}$ case (iii) is obviously equivalent with case (i) and does not add anything new.

(iv) $p \neq 0$, $q \neq 0$: This case is the focus of attention in this paper. It cannot be reduced to any of the three cases above and enables us to study the symplectic symmetry in a quantum chaotic system and its influence on the localization length.

B. Symmetries

The standard kicked rotor is invariant with respect to time reversal, parity, and conjugation, three symmetries denoted by $\hat{T}$, $\hat{P}$, and $\hat{C}$, respectively, and given by [22]

$$\begin{aligned}\hat{T}:&\quad t \to -t, \hat{l} \to -\hat{l},\quad \theta \to\ \ \theta\ ,\\ \hat{P}:&\quad t \to\ \ t, \hat{l} \to -\hat{l},\quad \theta \to -\theta\ ,\\ \hat{C}:&\quad t \to -t, \hat{l} \to\ \ \hat{l},\quad \theta \to -\theta.\end{aligned} \tag{2.6}$$

The conjugation symmetry $\hat{C}$ is the time reversal symmetry in the l representation [15]. Obviously, $\hat{C} = \hat{T}\circ\hat{P}$,

and $\hat{C}\hat{P}\hat{T} = 1$. Only the $\hat{P}$ symmetry yields a conserved quantum number since $\hat{P}$ is a unitary symmetry whereas $\hat{T}$ and $\hat{C}$ are antiunitary. The $\hat{C}$ symmetry, the "conjugation symmetry," is the most interesting of the three since it is perfectly suited for our investigation of localization phenomena in the symplectic kicked rotor model. This is so because $\hat{l} \to \hat{l}$ under the application of $\hat{C}$, which means that a rotor wave function localized at a site $l_0 \gg 0$ with localization length $\lambda \ll l_0$ will not be displaced on the l lattice under the application of $\hat{C}$, but stays localized around l_0. This enables us to work with a model space centered around l_0 and to neglect altogether the space $l < 0$. The restriction to the $l > 0$ model space is allowed since a wave packet started out localized around $l_0 \gg 0$ has only an exponentially small chance to tunnel into the space $l < 0$ under the dynamics defined by (2.1).

As a result and without loss of generality, we will from now on always assume that $l > 0$. In this case the time reversal symmetry $\hat{T}$ loses its meaning and the conjugation symmetry $\hat{C}$ takes its place as the only antiunitary symmetry which leaves the model space invariant. It was shown by Robnik and Berry [25] that any antiunitary symmetry can serve as a generalized time reversal symmetry. Thus the $\hat{C}$ symmetry enables us to study the effects of an antiunitary symmetry (and its breaking) on the localization length of the system.

It is well known [1,17,18,25] that the presence or absence of an antiunitary symmetry can change drastically global features of a quantum system even without affecting its classical properties. As an example, consider case (ii) in Sec. II A above. As discussed, it is equivalent with two spinless Hamiltonians each of which is equivalent with the spinless Hamiltonian discussed in Ref. [21]. Switching on the q parameter, the two decoupled spinless Hamiltonians cease to be invariant under $\hat{C}$ as defined in (2.6). As a consequence, the localization length of the system increases by a factor of 2. This fact was presented in Ref. [21] together with a thorough study of the symmetry-breaking region in the vicinity of $q = 0$.

In the case $p \neq 0$, $q \neq 0$ we need an extension of the $\hat{C}$ symmetry which can be applied in a case with spin. We use

$$\hat{C} = i\sigma_y \hat{P} \hat{K} , \tag{2.7}$$

where $\hat{K}$ is the operator of complex conjugation. It is then easy to see that $\hat{C}H\hat{C} = H$ for all p and q. At this point there seems to be a problem: How was it possible to study the destruction of the $\hat{C}$ symmetry in Ref. [21] whereas the Hamiltonian in Ref. [21] according to (ii) in Sec. II A above is only a special case of (2.1) for $p = 0$ and (2.1) is obviously invariant under $\hat{C}$ defined in (2.7) for all p and q? The answer is that on the spinless level, the $\hat{C}$ symmetry as defined in (2.6) is indeed destroyed. In the general case with spin, H is indeed $\hat{C}$ invariant for all p and q. But whereas $\hat{C}$ is the only symmetry of the problem for $p \neq 0, 1$, $q \neq 0, 1$, there is an additional "geometric" symmetry [18] in the case $p = 0$: $\hat{G} = i\sigma_x$ with $[\hat{G}, H] = 0$, $[\hat{G}, \hat{C}] = 0$, $\hat{G}^2 = -1$. This means that H no longer belongs to the symplectic universality class but exhibits the features of the unitary universality class, the case which was studied in Ref. [21]. A more detailed discussion of the statistical properties of H, for various choices of p and q will be presented in the following section.

C. Quasienergy statistics

In this section we present an effective way to characterize the symmetry of the Hamiltonian $\hat{H}$ as a function of p and q. For time periodic systems such as (2.1) it is possible to define the one-cycle propagator U which propagates the system over one complete period of the external perturbation. Since the dynamics of (2.1) can easily be obtained from powers of U, all the relevant dynamical information is in fact contained in U. In particular U and H share the same universality class. Therefore, instead of studying the symmetry properties of H, we can study the symmetry properties of U which are reflected in the statistics of the eigenphases of U, the quasienergies [26]. The statistical universality classes relevant for the quasienergy problem are Dyson's three circular ensembles (COE, CUE, and CSE) introduced above. All three ensembles show level repulsion on the unit circle and we expect that we can switch between these three universality classes as a function of the two symmetry-breaking parameters p and q. Since our model space is restricted to the $l > 0$ states, the one-cycle propagator U is nonreducible. Therefore, diagonalizing U in a finite basis (the number of basis states being denoted by B), we obtain the quasienergies which can be evaluated for their statistical properties. It is expected that in the spinless case [or in equivalent cases such as (iii) in Sec. II A above] and in the presence of an antiunitary symmetry, such as $\hat{C}$, the quasienergy statistics will be COE. In the spin-$\frac{1}{2}$ case, COE is obtained in the presence of two additional geometric symmetries. For broken $\hat{C}$ symmetry, or in the presence of one additional geometric symmetry in the spin-$\frac{1}{2}$ case, we expect CUE statistics. In the case of half-integer spin with only $\hat{C}$ active we expect to obtain CSE statistics. There is, however, one caveat. In the presence of localization the classification into the three universality classes and therefore the introduction of the Dyson β in (1.1) is meaningful only if the basis size B is smaller than the localization length. Only in this case will the quasienergy states interact strongly with each other and show level repulsion. In contrast, if $B >> \lambda$, eigenstates separated by more than the localization length λ can be accommodated in the basis. But since such states show only an exponentially small inhibition to level crossing, we expect to obtain Poissonian statistics independently of the symmetries present [27–29]. There is nothing wrong with $B < \lambda$ since the idea in this section is to construct an effective procedure for the characterization of the symmetry properties of H (U) rather than to obtain a converged representation for the rotor dynamics.

We found that for specific values (or ranges) of p and q the quasienergy statistics of U is indeed very well described by one of the three universality classes, while for some combinations of p and q the statistics is not well de-

scribed by either one of the three universality classes. We call these regions the "transition regions." A graphical representation of the mapping which assigns the respective symmetry class to a given (p,q) combination will be presented in the next section. Here we will focus on three specific combinations of p and q and exhibit the corresponding statistics of U.

Given p and q we calculated U for the Hamiltonian H defined in (2.1) [or (2.2), respectively] in a basis of size $B = 81$ states. For all three cases (a)–(c) discussed below we chose $\tau = \hat{\tau} = 0.05 \times 2\pi/g \approx 0.508$ where $g = (\sqrt{5}-1)/2 \approx 0.618$ denotes the "golden mean." The control parameter k in (2.1) was chosen such as to result in $\lambda \gg B$. The basis was centered around l_0 with 40 states to the left and 40 states to the right of l_0. The one-cycle propagator $\hat{U}$ was calculated for 151 values of l_0 ranging from $l_0 = 5000$ in steps of 100 to $l_0 = 20\,000$. The one-cycle propagators were diagonalized and the resulting quasienergy statistics were added up after appropriate normalization to the mean spacing. A similar set of calculations with $B = 161$ states confirmed the following results.

(a) For $p = 0$, $q = 0$, and $k = \hat{k} = 20/\hat{\tau} \approx 39.345$ we obtained the result shown in Fig. 1(a). The quasienergy statistics is very close to Wignerian statistics. Therefore U belongs to the COE universality class. This is natural since for $p = 0$, $q = 0$ the Hamiltonian H is equivalent with the spinless standard kicked rotor which is $\hat{C}$ invariant in the sense of (2.6). It is well known that in the presence of an antiunitary symmetry and in the spinless case COE is the expected universality class for the quasienergy statistics.

(b) Choosing $p = 0$ and $q = \frac{1}{2}$ the resulting quasienergy statistics is shown in Fig. 1(b). It is very close to CUE which is the expected universality class if a (generalized) time reversal symmetry is absent. Since case (b) corresponds to (ii) (Sec. II A above) which shows that H in this case is equivalent with the spinless Hamiltonian treated in Ref. [21], the $\hat{C}$ symmetry as defined in (2.6) is indeed destroyed and the result shown in Fig. 1(b) is consistent with our expectations.

(c) In case the spin-$\frac{1}{2}$ degree of freedom is nontrivially switched on, $\hat{C}$ as defined in (2.7) is the only symmetry of (2.1). In this case we expect symplectic quasienergy statistics. In order to check it we chose the representation (2.2) of the Hamiltonian H. For $\kappa = \hat{k}$, $\varepsilon = 0.3$, and $\mu = 0.8$ we obtained the result shown in Fig. 1(c). This result is very close to symplectic statistics and is again consistent with our expectations.

We conclude this section with a short note. Replacing the kinetic energy term in (2.1) by $\frac{1}{2}\tau\hat{l}^2 \to \frac{1}{2}\tau(\hat{l}+\gamma)^2$ does not change at all the statistical universality class of the Hamiltonian even if γ is not an integer. Although γ corresponds to the switching on of a "magnetic field" term which in other problems may destroy conventional time reversal symmetry, it is of no effect in our problem since, as mentioned above, the "time reversal" in our system is $\hat{C}$ which conserves $\hat{l}$. Just to make sure, we repeated the calculations leading to Figs. 1(a)–1(c) with $\gamma = g$. Figures 1(a)–1(c) remained unchanged under this

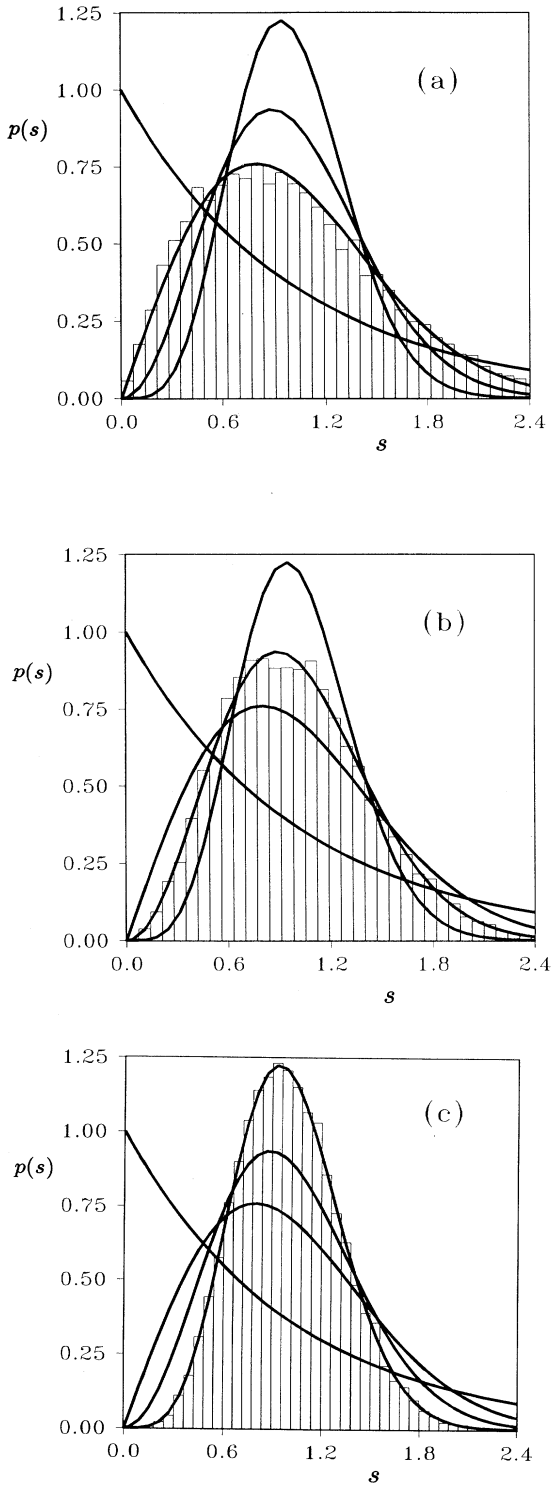

FIG. 1. Histogram: Quasienergy statistics of the one-cycle propagator of the generalized kicked rotor defined in (2.1). Basis size $B = 81$ states. We added up 151 statistically independent cases for better overall statistics. $\tau = \hat{\tau}$, (a) $(k,p,q) = (\hat{k},0,0)$; (b) $(k,p,q) = (\hat{k},0,\frac{1}{2})$; (c) $(\kappa,\varepsilon,\mu) = (\hat{k},0.3,0.8)$. The full lines correspond to Poissonian, COE, CUE, and CSE statistics, respectively.

modification. We emphasize, however, that noninteger γ indeed has a noticeable effect if one works with $l_0 = 0$ and in a basis which includes positive and negative angular momenta l. This case was studied by Izrailev [27], who showed that a nonzero γ indeed switches the quasienergy statistics from COE to CUE in a symmetric basis.

The different universality classes, which appear as p and q are varied, can loosely be interpreted as different "phases" of the Hamiltonian (2.1). In the next section we will present "phase diagrams" which graphically map (p, q) combinations onto the different statistical universality classes exhibited by U.

D. Phase diagrams

In the preceding section we saw that the one-cycle operator U of the Hamiltonian (2.1) has the potential to exhibit three different universality classes: COE, CUE, and CSE. Moreover, our computations showed that U switches smoothly between these three statistical classes as a function of the symmetry-breaking parameters p and q. Therefore an important piece of information about U is to know which statistical class U belongs to for a given choice of parameters. The best way to visualize this mapping is in the form of a two-dimensional chart which shows the different universality classes corresponding to the symmetry-breaking parameters in the form of a "phase diagram." In Ref. [21] it was found that the transition between COE and CUE happens very quickly as a function of the symmetry-breaking parameter q. For this reason, we choose to dilate the axes of the phase diagrams and define

$$x = \ln[p/(1-p)], \quad y = \ln[q/(1-q)] \quad . \tag{2.8}$$

For $\tau = \hat{\tau}$ and $k = \hat{k}$ the result is shown in Fig. 2(a). We can clearly distinguish five regions in the x, y parameter space denoted by Ia, Ib, IIa, IIb, and III, respectively. In regions Ia and Ib the quasienergy statistics of U is predominantly COE [denoted by the circles in Fig. 2(a)]. In regions IIa and IIb we have predominantly CUE statistics (crosses) and in region III the quasienergy statistics is predominantly CSE (triangles). The transition between the different regions is not abrupt. There is a transition region in which the quasienergy statistics is not close to either of the three standard cases. This is why we used the term "predominantly" above. In more detail it means the following: In order to find out which statistics is the appropriate one for a given combination of x and y (p and q, respectively), we calculated the quasienergy statistics of the one-cycle propagator according to the procedures stated in Sec. II C. The decision on the universality class was taken on the basis of the combined statistics of 151 matrices of size $B = 161$ for every single grid point shown in Fig. 2(a). The statistics obtained was represented as a histogram (see Fig. 1 for three special cases). Then, by computing χ^2 deviations, the shape of the histogram was compared with the theoretical expectations for the three universality classes (see full lines in Fig. 1). Every point (p, q) on the grid of Fig. 2(a) was then assigned a plot symbol representing the statistics which yielded the smallest χ^2 for the histogram corresponding to (p, q).

Clearly the type of "either/or" decision used in selecting the statistical class for given (p, q) is not able to say anything about the quality of the fits. This means that Fig. 2(a) does not give any information about the widths of the transition regions.

Qualitatively the occurrence and location of the five different "phases" in Fig. 2(a) can be understood very well. For instance, the region in which x and y are both large and negative corresponds to both p and q small. This is equivalent with the standard kicked rotor and accompanying COE statistics. Increasing y, corresponding to an increase of q, we enter region IIa which corresponds to CUE statistics. This case was discussed in Ref. [21]. At $y \approx 5$ we switch back to COE. This is natural because for large y, $q \to 1$, which means that for small p there is essentially only the term proportional to σ_x switched on in (2.1). In the representation in which σ_x is diagonal, this is equivalent with a standard $\sin(2\theta)$ kicked rotor. Therefore COE is the expected statistics. Similar arguments can be put forward to explain the locations of the rest of the Ia phase and the IIb phase. Phase III, the

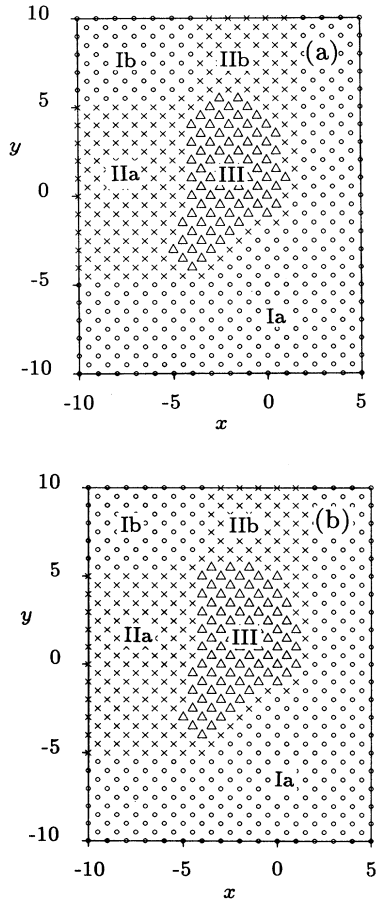

FIG. 2. Phase diagrams exhibiting the switching between different universality classes as a function of x and y. $\tau = \hat{\tau}$ and (a) $k = \hat{k}$; (b) $k = 51.75$. The circles, crosses, and triangles correspond to COE, CUE and CSE, respectively.

symplectic region, is naturally located at the center of Fig. 2(a) which corresponds to strong coupling between all degrees of freedom in (2.1).

Figure 2(b) shows the phase diagram for $k = 51.75$. It is very similar to Fig. 2(a) where we used $k = \hat{k} \approx 39.345$. Thus the two figures indicate that the borderlines between the different universality classes are essentially determined by the symmetry-breaking parameters p and q and only weakly dependent on k.

III. THE CUE LIMIT

The purpose of this section is a thorough discussion of the CUE limit of the Hamiltonian (2.1), i.e., $p = 0$, $q \neq 0$. First results for this case were already reported in Ref. [21]. Here we will attempt a clearer and more detailed exposition. Also, new results will be presented. For $p = 0$ and in the representation in which σ_x is diagonal the Hamiltonian (2.1) is equivalent with

$$H = \tfrac{1}{2}\tau\hat{l}^2 + k\, f_q(\theta)\, \delta_p(t), \tag{3.1}$$

where

$$f_q(\theta) = \cos\left(\frac{\pi q}{2}\right)\cos(\theta) + \tfrac{1}{2}\sin\left(\frac{\pi q}{2}\right)\sin(2\theta) \quad . \tag{3.2}$$

This is the Hamiltonian which will be used throughout this section. The classical dynamics induced by the Hamiltonian (3.1) is chaotic for sufficiently large $K = k\tau$. The form of the Hamiltonian is such that in the limit of large K the diffusion constant $D(K,q)$ is independent of q. For any finite value of K the ratio $R(K,q) = D(K,q)/(K^2/2)$ can be approximated by an analytical expression which will be derived in the following section. As was pointed out in the Introduction, a precise knowledge of the classical diffusion constant is mandatory for a meaningful comparison of localization lengths obtained in different symmetry regimes.

A. Classical diffusion

The diffusion constant for (3.1) can be calculated analytically with the help of a method due to Rechester and White [19] and Rechester, Rosenbluth, and White [20]. Although their analysis applies to the case $q = 0$ it is straightforward to extend their calculations to the case $q \neq 0$. According to (17) in Ref. [19] we have

$$D(K,q) = \lim_{T\to\infty} \frac{1}{T} \sum_{m_T=-\infty}^{\infty} \cdots \sum_{m_1=-\infty}^{\infty} \left[\prod_{i=0}^{T} \int_0^{2\pi} \frac{d\theta_i}{2\pi}\right] S_{T-1}^2(K,q) \times \exp\left\{\sum_{j=1}^{T} i m_j[\theta_j - \theta_{j-1} - S_{j-1}(K,q)]\right\} , \tag{3.3}$$

with

$$S_j = K \sum_{p=0}^{j} f_q(\theta_p) \quad . \tag{3.4}$$

Note that we define D as being normalized to $K^2/2$ for large K. Also, we use S_{T-1} instead of S_T which is a matter of convention. The representation (3.3) for $D(K,q)$ can be expressed as a sum of products of Bessel functions. The lowest-order products are obtained by keeping the following terms in the sum (3.3): (i) $m_l = 0, l = 1,...,T$; (ii) $m_{l-1} = -m_l, m_l = \pm 1 \pm 2, l = 2,3,...,T$; (iii) $m_{l-2} = -m_l, m_l = \pm 1 \pm 2, l = 2,3,...,T$; (iv) $m_{l-2} = m_l, m_{l-1} = -2m_l, m_l = \pm 1 \pm 2, l = 3,4,...,T$. The evaluation of the integrals in (3.3) for the cases (i)–(iv) is lengthy but elementary. The final result is

$$R(K,q) = \frac{D(K,q)}{(K^2/2)} \approx 1 + 2\sum_{i=1}^{6} R_i(K,q) \, , \tag{3.5}$$

with

$$R_1 = -\cos^2\left(\frac{\pi q}{2}\right)\left\{J_0(\sigma)J_2(\gamma) + \sum_{M=1}^{\infty}(-1)^M J_{2M}(\sigma)[J_{4M-2}(\gamma) + J_{4M+2}(\gamma)]\right\} ,$$

$$R_2 = \sin^2\left(\frac{\pi q}{2}\right)\left\{J_0(2\sigma)J_4(2\gamma) + \sum_{M=1}^{\infty}(-1)^M J_{2M}(2\sigma)[J_{4M-4}(2\gamma) + J_{4M+4}(2\gamma)]\right\} ,$$

$$R_3 = -\cos^2\left(\frac{\pi q}{2}\right)\left\{\left[J_1(\gamma)J_0(\sigma) + \sum_{M=1}^{\infty}(-1)^M J_{2M}(\sigma)[J_{4M+1}(\gamma) - J_{4M-1}(\gamma)]\right]^2 - \left[\sum_{M=1}^{\infty}(-1)^M J_{2M-1}(\sigma)[J_{4M-1}(\gamma) - J_{4M-3}(\gamma)]\right]^2\right\} , \tag{3.6}$$

$$R_4 = \sin^2\left(\frac{\pi q}{2}\right)\left\{\left[J_2(2\gamma)J_0(2\sigma) + \sum_{M=1}^{\infty}(-1)^M J_{2M}(2\sigma)[J_{4M-2}(2\gamma) + J_{4M+2}(2\gamma)]\right]^2 - \left[\sum_{M=1}^{\infty}(-1)^M J_{2M-1}(2\sigma)[J_{4M-4}(2\gamma) + J_{4M}(2\gamma)]\right]^2\right\},$$

$$R_5 = \cos^2\left(\frac{\pi q}{2}\right)\left\{\left[J_3(\gamma)J_0(\sigma) - J_2(\sigma)\,[J_5(\gamma) + J_1(\gamma)] + \sum_{M=2}^{\infty}(-1)^M J_{2M}(\sigma)[J_{2M+3}(\gamma) - J_{2M-3}(\gamma)]\right]^2 + \left[\sum_{M=2}^{\infty}(-1)^M J_{2M-1}(\sigma)\,[J_{4M+1}(\gamma) - J_{4M-5}(\gamma)] - J_1(\sigma)\,[J_5(\gamma) + J_1(\gamma)]\right]^2\right\},$$

$$R_6 = \sin^2\left(\frac{\pi q}{2}\right)\left\{\left(J_6(2\gamma)J_0(2\sigma) - J_2(2\sigma)\,[J_{10}(2\gamma) + J_2(2\gamma)] + \sum_{M=2}^{\infty}(-1)^M J_{2M}(2\sigma)[J_{4M+6}(2\gamma) + J_{4M-6}(2\gamma)]\right)^2 + \left[-J_1(2\sigma)[J_8(2\gamma) + J_4(2\gamma)] + \sum_{M=2}^{\infty}(-1)^M J_{2M-1}(2\sigma)\,[J_{4M+4}(2\gamma) + J_{4m-8}(2\gamma)]\right]^2\right\}.$$

We defined $\sigma = K\sin(\pi q/2)$ and $\gamma = K\cos(\pi q/2)$. Two special cases of (3.5) are of interest. For $q = 0$ (3.5) reduces to [19]

$$R(K, q = 0) = 1 - 2J_2(K) - 2J_1^2(K) + 2J_3^2(K) \quad . \quad (3.7)$$

For $q = 1$ we obtain

$$R(K, q = 1) = 1 - 2J_2(2K) - 2J_1^2(2K) + 2J_3^2(2K). \quad (3.8)$$

It is illustrative to expand (3.7) and (3.8) to the first nontrivial order in K. We obtain

$$R(K, q = 0) \sim 1 \; - \; 2\sqrt{\frac{2}{\pi K}}\cos\left(K - \frac{5\pi}{4}\right), \quad (3.9)$$

$$R(K, q = 1) \sim 1 \; - \; 2\sqrt{\frac{1}{\pi K}}\cos\left(2K - \frac{5\pi}{4}\right) \quad . \quad (3.10)$$

In both cases $R(K, q) \sim 1$ for large K and is independent of q. At $q = 1$ the oscillations in R as a function of K appear at twice the frequency as compared with the case $q = 0$.

The quality of the result (3.5) can be appreciated in Fig. 3 where for $K = 20$ we compare the analytical result (3.5) (solid line) with the results of a Monte Carlo simulation (bullets). Figure 4 shows a similar comparison but as a function of K for fixed $q = 0.2$ [Fig. 4(a)] and $q = 0.5$ [Fig. 4(b)]. The numerical Monte Carlo data displayed in Figs. 3 and 4 are obtained on the basis of 200 000 simultaneously propagated classical trajectories initially equidistributed in the angle variable θ. The statistical error of the classical calculations is less than the size of the dots in Figs. 3 and 4.

At certain places in Figs. 3 and 4 large deviations between the result (3.5) and the numerically obtained diffusion constants can be seen. These deviations are due to accelerator modes [23]. Accelerator modes in the Hamiltonian (3.1) are apparently very important. We found that for certain (K, q) combinations accelerator islands can occupy θ intervals up to 5% even at $K \approx 20$.

B. Semiclassical theory

A convenient tool for the study of localization and its relation to the underlying classical diffusion is the *mean staying probability* $P_s(n)$ defined as the probability to remain in the "site" l_0 after the application of n kicks averaged over a large domain of l_0 values [22]:

$$P_s(n) = \lim_{\Delta\to\infty}\frac{1}{\Delta}\sum_{l_0=-\Delta/2}^{\Delta/2}|\langle l_0|U^n|l_0\rangle|^2 \quad . \quad (3.11)$$

In the semiclassical limit ($k \to \infty$, $\tau \to 0$, $K = k\tau$ fixed) this function has the following properties [22]: (i) There

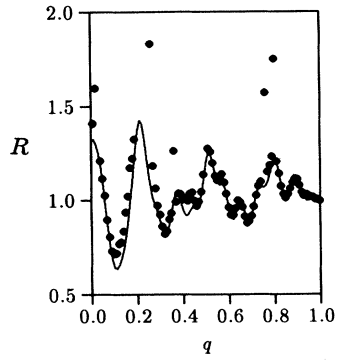

FIG. 3. The normalized diffusion constant R as a function of the symmetry-breaking parameter q for $p = 0$ and $K = 20$. Solid line: Analytical result. Circles: Classical Monte Carlo calculation. Sporadically occurring large discrepancies between the Monte Carlo results and the analytical results are due to accelerator modes.

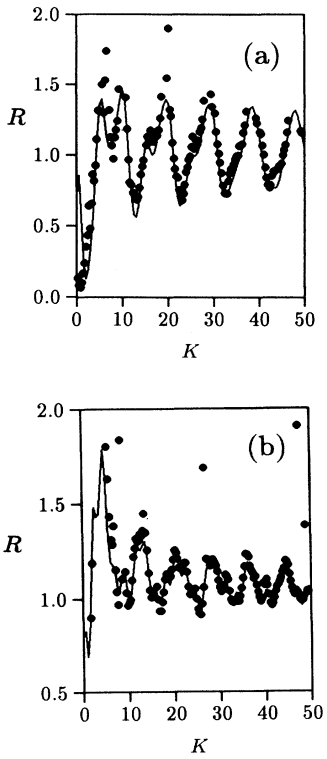

FIG. 4. Same as Fig. 3 but as a function of K for fixed q. (a) $q = 0.2$, (b) $q = 0.5$.

exists a critical time n^* such that for $n \gg n^*$ $P_s(n)$ approaches a constant value which equals the mean inverse participation ratio ξ^{-1}. For $1 < n \ll n^*$, $P_s(n)$ is proportional to the classical probability to stay. The proportionality factor depends on the symmetry of the Hamiltonian, and its value is 2 for the standard ($q = 0$) kicked rotor. (ii) For $q = 0$, $P_s(n)$ was shown to be a *scaling* function, such that

$$P_s(n) = \xi^{-1} f(n/\xi) \quad . \tag{3.12}$$

$f(x)$ is a universal function which interpolates between $f(x) \approx x^{-1/2}$ behavior for $x < 1$ and $f(x) \approx 1$ for $x > 1$. The scaling behavior incorporates the well-known relations [4,8,11] $n^* \sim \xi$ and $\xi \sim D$ and the proportionality between the localization length λ and the participation ratio ξ for exponentially localizing systems.

The function $P_s(n)$ distinguishes clearly between the two relevant time domains of the evolution. The $n < n^*$ domain is diffusive, and the classical dynamics dominates. The only remnant of quantum mechanics is the "weak localization" enhancement to be discussed below. The $n > n^*$ domain is dominated by strong localization, a purely quantum (wave) phenomenon. It is natural to seek a semiclassical theory to describe $P_s(n)$, and use it to interpolate between the two regimes. The semiclassical expression for $P_s(n)$ reads

$$P_s^{(\mathrm{SC})}(n) = \left\langle \left| \sum_\alpha p_\alpha^{1/2} \exp(iS_\alpha) \right|^2 \right\rangle \quad , \tag{3.13}$$

where the sum extends over all classical trajectories (denoted by α) which start at a given value of the angular momentum l and return to it after n kicks: $l_\alpha(0) = l_\alpha(n) = l$ (returning trajectory). The action accumulated along the trajectory is

$$S_\alpha(n) = \sum_{i=0}^{n-1} [\tfrac{1}{2}\tau l_{i+1}^2 - k\, f_q(\theta_i)] - l_0(\theta_n - \theta_0) \; - \; \frac{\pi}{2}\nu_\alpha \; , \tag{3.14}$$

with $f_q(\theta)$ defined in (3.2). The action is measured in units of $\hbar$, and ν_α is the Maslov index. p_α in (3.13) is the contribution of the trajectory α to the classical staying probability, $p_\alpha = \frac{1}{2\pi}|dl_\alpha(n)/d\theta_\alpha(0)|^{-1}$. The angular brackets denote averaging on l_0 as in (3.11).

If the Hamiltonian is invariant under a symmetry operation *which does not affect the boundary conditions* $l_\alpha(0) = l_\alpha(n) = l$, as is the case with the returning trajectories defined above, then to any trajectory α we can assign a conjugate trajectory α_c by applying the symmetry operation to a trajectory. Among the symmetry operations listed above, only $\hat{C}$ provides a relevant conjugation, since this is the only operation which preserves the sign of $\hat{l}$.

Consider, e.g., the standard kicked rotor [$q = 0$ in (3.1)]. The dynamics of the standard kicked rotor is described by the standard mapping

$$\begin{aligned} l_{n+1} &= l_n + k \sin(\theta_n) \; , \\ \theta_{n+1} &= \theta_n + \tau\, l_{n+1} \quad . \end{aligned} \tag{3.15}$$

Given the initial conditions (θ_0, l_0) of a classical trajectory α, the mapping (3.15) allows one to calculate the values of the trajectory at arbitrary times n. If α: (θ_j, l_j), $j = 0, 1, ..., N$ is a solution of the standard mapping (3.15) so is the $\hat{C}$ conjugated trajectory α_c : (ϑ_j, L_j), $j = 0, ..., N$ with

$$L_j = l_{N-j}, \quad \vartheta_j = -\theta_{N-j-1} \; , \tag{3.16}$$

and $\vartheta_N = \tau l_0 - \theta_0$. Since for $q = 0$ every returning trajectory α possesses an associated conjugate trajectory α_c, (3.13) can be written as

$$P_s^{(\mathrm{SC})}(n) = 4\left\langle \left| {\sum_\alpha}' p_\alpha^{\frac{1}{2}}(n) e^{iS_\alpha(n)} \right|^2 \right\rangle_{l_0} \; , \tag{3.17}$$

where $\sum'$ denotes summation over returning trajectories excluding their conjugates. Especially for short trajectories (small N) it can happen that a trajectory α equals its conjugate trajectory, i.e., $\alpha = \alpha_c$ (self-conjugate trajectory). In this case the conjugate trajectory does not give rise to a factor of 2 in the amplitude since otherwise the trajectory α would be double counted in (3.17). Self-conjugacy, however, becomes progressively more rare as the length of the trajectory, N, increases.

Suppose now that q is small enough so that the labels α and α_c can still be used to identify trajectories which were exactly conjugate at $q = 0$. In this case $p_\alpha(q) \approx p_{\alpha_c}(q) \approx$

$p_\alpha(q=0)$ is an acceptable approximation. The actions S_α and S_{α_c}, however, change in different directions which leads to interference terms in (3.17). We have

$$S_\alpha(n,q) = S_\alpha(n,0) - \delta_\alpha(n) \ , \qquad (3.18)$$
$$S_{\alpha_c}(n,q) = S_\alpha(n,0) + \delta_\alpha(n) \ ,$$

with

$$\delta_\alpha(q) = \frac{k}{2}\sin\left(\frac{\pi q}{2}\right)\sum_{i=0}^{n-1}\sin(2\theta_i^{(\alpha)}) \quad . \qquad (3.19)$$

Therefore the staying probability (3.17) is now given by

$$P_s^{(\mathrm{SC})}(n;q) = 4\left\langle {\sum_\alpha}' p_\alpha(n)\cos^2\delta_\alpha(n)\right\rangle_{l_0} + 4\left\langle {\sum_{\alpha\neq\beta}}' p_\alpha^{\frac{1}{2}}(n)p_\beta^{\frac{1}{2}}(n)e^{i(S_\alpha-S_\beta)}\cos\delta_\alpha(n)\cos\delta_\beta(n)\right\rangle_{l_0} . \qquad (3.20)$$

The first term in (3.20) is the "diagonal" contribution to the staying probability. It can be written as $P_s^{(D)}(n;q) = \langle 2\cos^2\delta(n;q)\rangle P_s^{(\mathrm{cl})}(n;q)$ where, besides the l_0 average, the angular brackets denote a weighted average over classical staying probabilities and $P_s^{(\mathrm{cl})}(n;q) = 2{\sum_\alpha}' p_\alpha$ is the total classical probability to stay. According to (3.19) the phase δ is a sum of n terms. Therefore, for chaotic systems, and assuming statistical independence of the successive $\sin(2\theta_i^{(\alpha)})$, the phases δ in the limit of large n form a Gaussian ensemble with vanishing mean and with variance $\langle\delta^2\rangle = \frac{n}{2}[\frac{k}{2}\sin(\frac{\pi q}{2})]^2$. Hence,

$$P_s^{(D)}(n;q) = P_s^{(\mathrm{cl})}(n)F(k,q;n)$$
$$= P_s^{(D)}(n;q=0)F(k,q;n)/2 \ , \qquad (3.21)$$

with $F(k,q;n) = \left\{1+\exp[-n\frac{k^2}{4}\sin^2(\frac{\pi q}{2})]\right\}$. For small values of n, the nondiagonal contribution in (3.20) vanishes upon averaging and the probability to stay is entirely dominated by (3.21). Here, the quantal probability differs from its classical counterpart by a smooth function of time which depends upon the symmetry-breaking parameter q in a way which interpolates smoothly between the limits 2 (for $q=0$) and 1 for large q. The factor 2 is the typical "weak localization" enhancement which is known in many fields of physics [30 – 35]. It is due to the invariance of the system under a symmetry of the type described above.

The diagonal contribution to the staying probability vanishes as $n^{-1/2}$. Hence, the long time properties of $P_s(n)$ are due exclusively to the nondiagonal contribution in the semiclassical expression (3.20). This is the semiclassical manifestation of the well-known fact that localization [here, finite value of $P_s(n), n > n^*$] is due to genuine quantum interference effects, and has no classical analog. In spite of its importance for the semiclassical computation of the localization length, the evaluation of the nondiagonal sum continues to form an unsolved problem. To demonstrate the dangers of a simplistic approach to this sum let us try some commonly used intuition which works reasonably well for $n < n^*$ but leads to an erroneous result for $n > n^*$. For $n < n^*$ one can argue that contributions to the nondiagonal term are expected to come from pairs of trajectories α and β whose action differences are small. Hence, one may extract from the nondiagonal term a $\langle\cos^2\delta\rangle_{\mathrm{av}}$ term in much the same manner as was done for the diagonal sum:

$$P_s^{(\mathrm{ND})}(n,q) \approx P_s^{(\mathrm{ND})}(n;q=0)F(k,q;n) \quad . \qquad (3.22)$$

Combining (3.21) and (3.22) we find the following result:

$$P_s(n,q) \approx P_s(n;q=0)F(k,q;n) \quad . \qquad (3.23)$$

For $n > n^*$, however, this line of argumentation does not correctly take the interference terms in the nondiagonal sums into account. It does not include effects of localization which for small q are responsible for saturating the staying probability $P_s(n,q)$ at levels much higher than predicted by (3.23). We will show this fact in the following section (see especially Fig. 5).

C. Quantum calculations

In order to check our semiclassical predictions we calculated exact quantum mechanical staying probabilities for the symmetry-broken kicked rotor defined in (3.1) for various values of q. The rotor wave functions were propagated using the standard fast Fourier technique [3,5,24]. For $\tau = \hat{\tau}$ and $k = \hat{k}$ the resulting staying probabilities were averaged over 390 l_0 values, $l_0 = 1000i + j$, $i = 1, ..., 30$, $j = -6, ..., +6$. For $n < n^*$ we find excellent agreement between (3.23) and our numerical simulations (see Fig. 5).

The dependence of P_s on q as shown in Fig. 5 and resulting (for $n < n^*$) from the presence of the F function in (3.23) is due exclusively to the effect of breaking an antiunitary symmetry and has nothing to do with the fact that an additional perturbation is switched on. Therefore a crucial test of (3.23) is provided by replacing the $\sin(2\theta)$ function in (3.1) by $\cos(2\theta)$. In this case we expect $P_s(n;q) = P_s(n;q=0)$ since the $\hat{C}$ symmetry is not broken in this case [36]. This is confirmed by our numerical results (dashed ragged line in Fig. 5). Thus this numerical experiment, which we call the "$\cos(2\theta)$ test," shows unambiguously that the q-dependent reduction in P_s is "real" and has to be attributed entirely to the breaking of an antiunitary symmetry. It cannot be explained as an artifact caused by a small additional interaction term.

For large n values (3.23) implies that an arbitrarily small symmetry-breaking perturbation will cause the staying probability to decrease to half its value at $q=0$ after sufficiently long time. Figure 5 shows that (3.23)

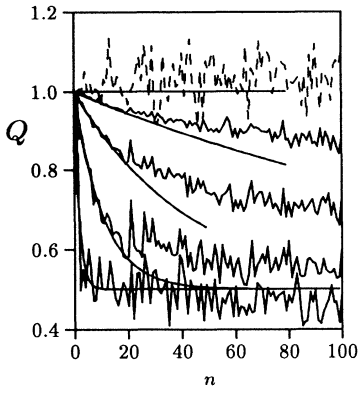

FIG. 5. Normalized staying probabilities $Q(n,q) = P_s(n,q)/P_s(n,q=0)$. Full ragged lines: quantum results for $q = 0.005, 0.01, 0.02, 0.05$. Smooth solid lines: the semiclassical prediction (3.23). Dashed ragged line: quantum result for the "cos(2θ) test" (see text).

is not valid for $n > n^*$. In other words, the simple-minded argument which led us to (3.23) cannot be used for $n > n^*$. Rather, our numerical work suggests that due to strong localization $P_s(n;q)$ freezes at $n \approx n^*$ and the asymptotic value of $P_s(n;q)$ is given approximately by

$$P_a(q) \equiv \lim_{N\to\infty} \frac{1}{N-n^*} \sum_{n=n^*+1}^{N} P_s(n;q) = P_a(q=0)F(k,q;\nu n^*) \quad , \tag{3.24}$$

where ν is a numerical factor on the order of 1. If so, then (3.24) predicts that for small q and with $n^* \sim D \sim k^2$, the ratio $Q_a \equiv P_a(q)/P_a(q=0)$ scales in $z \equiv q^2k^4$. Apart from statistical and possibly systematic fluctuations this is indeed the case (see Fig. 6).

When $k\sin(\pi q/2)/2 > 1$ we are in the extreme broken symmetry regime where $P_s(n;q) = P_s(n,0)/2$ for all n values. Here, $\xi(\beta) = \beta\xi(\beta=1)$. This is equivalent to what is known from the random-matrix treatment of localization in quasi-one-dimensional disordered systems

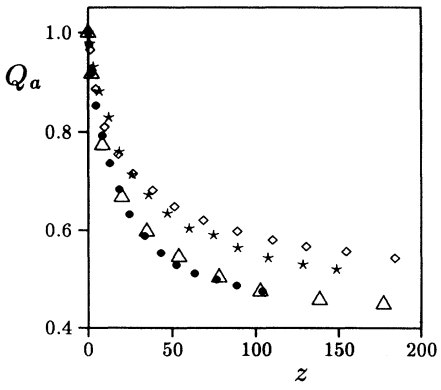

FIG. 6. Check of the scaling behavior of (3.24) for $k = 23.42$ (triangles), 19.67 (diamonds), 17.88 (stars), and 16.39 (bullets) for various values of q.

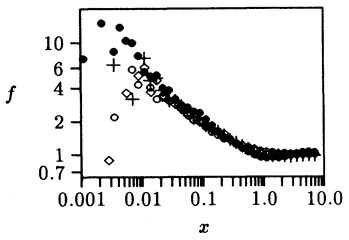

FIG. 7. The universal function $f(x) = \xi P_s(n)$ as a function of scaled time $x = \beta n/\xi(\beta=1)$ for $\beta = 1$ ($q = 0$, circles), $\beta = 2$ ($q = 0.32$, crosses; $q = 0.5$, diamonds, respectively), and $\tau = \hat{\tau}$, $k = \hat{k}$. The bullets correspond to the symplectic case ($\beta = 4$). Here, $\kappa = \hat{k}$, $\varepsilon = 0.3$, and $\mu = 0.8$.

[13,14]. Our numerical data suggest an even stronger result. We find that in the symmetry-broken regime the function $P_s(n;\beta)$ scales as

$$P_s(n;\beta) = \frac{1}{\xi(\beta)} f\left(\frac{\beta n}{\xi(\beta)}\right) , \tag{3.25}$$

where the function $f(x)$ is the same function as defined for the time reversal symmetric case (see Fig. 7). This result is surprising because of the following reason: It was shown in Ref. [22] that $P_s(n)$ is a Fourier transform of the two-point cluster function for the local spectral density. In (3.25) the *same* function is used for the correlation functions in the $\beta = 1$ or 2 ensembles. For the Dyson ensembles this is not the case, and the two cluster functions cannot be related by a simple scaling law.

A prerequisite for any scaling function of the type (3.25) is that the participation ratio and the classical diffusion constants are proportional. Only in this case is normalization of the localization lengths to the classical diffusion constants a meaningful procedure. Indeed, it was shown in Ref. [21] that the ratio $R^{(\mathrm{QM})}(k,\tau,q) = \xi(q)/2\xi(q=0)$ is close to unity on average, and that it fluctuates in a way which is rather similar to the corresponding ratio of the classical diffusion constants. This guarantees that the normalization to the classical diffusion constant ensures a common basis with respect to which the appearance of nontrivial factors in the localization length can be discussed.

IV. THE GENERAL CASE: CSE

We will now turn to the general case $p \neq 0$, $q \neq 0$ where the spin degrees of freedom in (2.1) are nontrivially switched on. According to the discussion in Sec. II this is the case where we expect the one-cycle operator U to exhibit CSE statistics if p and q are chosen from region III in Fig. 2. This case corresponds to $\beta = 4$ and offers the opportunity to check whether the localization length, as predicted by (1.1), really grows by a factor of 4 in this case.

Again, the importance of the classical diffusion constant has to be emphasized. Changing the symmetry-breaking parameters will in general result in a change

in the classical diffusion properties of the system. Obviously, the localization lengths for different universality classes can be compared with each other in a meaningful way only if the localization lengths are properly normalized to the corresponding classical diffusion constants. In order to calculate the diffusion constants we need a classical analog for the Hamiltonian (2.1) which is applicable for general p and q. Although the Hamiltonian (2.1) is spin dependent in the general case, a classical analog could be constructed easily in the preceding section because for $p = 0$ the Hamiltonian (2.1) can be naturally diagonalized and split into two decoupled rotors. Each one of the rotors, the "spin-up" rotor and the "spin-down" rotor, has a natural classical analog which is the parity broken kicked rotor. But in the most general case ($p \neq 0$, $q \neq 0$) the spin degrees of freedom are nontrivially coupled and it can be expected that the construction of a "classical" analog for the quantum Hamiltonian (2.1) is difficult. This is so because the spin expectation value is small ("spin-$\frac{1}{2}$ rotor") and by no means "classical." Therefore we construct a "classical" model by leaving the spin degrees quantum mechanical and going to the classical limit in the (n, θ) coordinates. In the following two sections we will propose two procedures, the mean-field approach and the Hamiltonian approach, respectively, which implement this program. They yield identical expressions for what could be called the classical mapping equations for the quantum Hamiltonian (2.1).

A. The mean-field approach

The essence of the mean-field approach is to replace the operators $\hat{l}$ and $\hat{\theta}$ in (2.1) with their expectation values. In order to derive the mean-field equations we start with the Hamiltonian (2.1) in the form (2.2) and assume that the total wave function $|\varphi(t)\rangle$ of the system can be factorized into a space part $|\psi\rangle$ and a spin part $|\chi\rangle$, with $\langle\psi \mid \psi\rangle = 1$ and $\langle\chi \mid \chi\rangle = 1$. This is obviously a problematic assumption since in our system the space and the spin degrees of freedom are strongly coupled. Despite its shortcomings we will use the mean-field approach in order to explore its consequences. Inserting $|\varphi\rangle = |\psi\rangle|\chi\rangle$ into the time-dependent Schrödinger equation $i\frac{\partial}{\partial t}|\varphi\rangle = H|\varphi\rangle$ we get

$$i\{|\dot{\psi}\rangle + \langle\chi \mid \dot{\chi}\rangle \mid \psi\rangle\} = \{\tfrac{1}{2}\tau\hat{l}^2 + \kappa\cos(\theta)\delta_p(t)\} \mid \psi\rangle + \kappa\{\tfrac{1}{2}\mu\sin(2\theta)\langle\chi \mid \sigma_x \mid \chi\rangle + \varepsilon\sin(\theta)\langle\chi \mid \sigma_z \mid \chi\rangle\}\delta_p(t) \mid \psi\rangle \ , \tag{4.1}$$

$$i\left\{\langle\psi \mid \dot{\psi}\rangle \mid \chi\rangle + \mid \dot{\chi}\rangle\right\} = \langle\psi \mid [\tfrac{1}{2}\tau\hat{l}^2 + \kappa\cos(\theta)\delta_p(t)] \mid \psi\rangle \mid \chi\rangle + \varepsilon\kappa\langle\psi \mid \sin(\theta) \mid \psi\rangle\delta_p(t)\sigma_z \mid \chi\rangle + \tfrac{1}{2}\mu\kappa\langle\psi \mid \sin(2\theta) \mid \psi\rangle\delta_p(t)\sigma_x \mid \chi\rangle \ . \tag{4.2}$$

We observe now that $\langle\psi|\dot{\psi}\rangle$ is purely imaginary and a function of time only. Furthermore, $\langle\psi|\frac{1}{2}\tau\hat{l}^2 + k\cos(\theta)\delta_p(t)|\psi\rangle$ is only a function of time. Inserting the gauge transformation

$$|\chi\rangle = \exp\left\{-i\int_0^t [\langle\psi \mid \tfrac{1}{2}\tau\hat{l}^2 + \kappa\cos(\theta)\delta_p(t') \mid \psi\rangle - i\langle\psi \mid \dot{\psi}\rangle]dt'\right\} \mid \phi\rangle \tag{4.3}$$

into (4.2) yields

$$i \mid \dot{\phi}\rangle = \varepsilon\kappa\langle\psi \mid \sin(\theta) \mid \psi\rangle\delta_p(t)\sigma_z \mid \phi\rangle + \tfrac{1}{2}\mu\,\kappa\langle\psi \mid \sin(2\theta) \mid \psi\rangle\delta_p(t)\sigma_x \mid \phi\rangle \ . \tag{4.4}$$

A similar gauge transformation

$$|\psi\rangle = \exp\left\{-\int_0^t \langle\chi \mid \dot{\chi}\rangle dt'\right\} \mid \alpha(t)\rangle \tag{4.5}$$

inserted into (4.1) yields

$$i\frac{\partial}{\partial t}|\alpha\rangle = \tilde{H}|\alpha\rangle \ , \tag{4.6}$$

with

$$\tilde{H} = H_0 + V(t) \ , \tag{4.7}$$

where

$$H_0 = \tfrac{1}{2}\tau\hat{l}^2 + \kappa\cos(\theta)\delta_p(t) \tag{4.8}$$

and

$$V(t) = \kappa[\varepsilon\sin(\theta)\langle\phi \mid \sigma_z \mid \phi\rangle + \tfrac{1}{2}\mu\sin(2\theta)\langle\phi \mid \sigma_x \mid \phi\rangle]\delta_p(t) \mid \alpha\rangle \ . \tag{4.9}$$

Equation (4.6) is nothing but a Schrödinger equation for $|\alpha\rangle$ with a Hamiltonian $\tilde{H}$ which can be immediately interpreted as a classical Hamiltonian. Introducing the notation $\langle\uparrow|\phi\rangle = \phi^{\uparrow}(t)$ and $\langle\downarrow \mid \phi\rangle = \phi^{\downarrow}(t)$, the classical equations of motion for l and θ are therefore given by

$$\dot{\theta} = \tau l \ , \tag{4.10}$$

$$\dot{l} = \kappa\{\sin(\theta) - \varepsilon\cos(\theta)[|\phi^{\uparrow}|^2 - |\phi^{\downarrow}|^2] - \mu\cos(2\theta)\,[\phi^{\uparrow *}\phi^{\downarrow} + \phi^{\downarrow *}\phi^{\uparrow}]\}\,\delta_p(t) \ . \tag{4.11}$$

In order to close Eqs. (4.11) we need $\dot{\phi}^{\uparrow}$ and $\dot{\phi}^{\downarrow}$. At this point we interpret θ as a classical variable. Accordingly, we approximate $\langle\psi|\sin(\theta)|\psi\rangle \sim \sin(\theta)$ and $\langle\psi|\sin(2\theta)|\psi\rangle \sim \sin(2\theta)$ and obtain from (4.4)

$$i\dot{\phi}^{\uparrow}(t) = \kappa\left\{\varepsilon\sin(\theta)\phi^{\uparrow}(t) + \frac{\mu}{2}\sin(2\theta)\phi^{\downarrow}(t)\right\}\delta_p(t)\ ,$$
$$i\dot{\phi}^{\downarrow}(t) = \kappa\left\{-\varepsilon\sin(\theta)\phi^{\downarrow}(t) + \frac{\mu}{2}\sin(2\theta)\phi^{\uparrow}(t)\right\}\delta_p(t). \tag{4.12}$$

Before presenting the mapping which corresponds to (4.10)–(4.12) (see Sec. IV C below) we will now derive the system of equations (4.10)–(4.12) from a different point of view.

B. The Hamiltonian approach

Just like in the preceding section our starting point is again the Hamiltonian (2.1) in its form (2.2). Suppose that l and θ in (2.2) are c numbers whose time dependence is given as $l(n)$ and $\theta(n)$. Then, the Hamiltonian (2.2) is the Hamiltonian of a spin-$\frac{1}{2}$ particle with

$$i\dot{\psi} = H\psi\ , \qquad \psi = \begin{pmatrix}\psi^{\uparrow}(l,\theta)\\ \psi^{\downarrow}(l,\theta)\end{pmatrix}\ . \tag{4.13}$$

Separating real and imaginary parts of $\psi^{\uparrow}$ and $\psi^{\downarrow}$ we define

$$\psi^{\uparrow} = A + iB\ ,\ \psi^{\downarrow} = C + iD\ . \tag{4.14}$$

Furthermore, we define the matrix elements of H as

$$\begin{aligned} H_{\uparrow\uparrow} &= \langle\uparrow|\ H\ |\uparrow\rangle = \tfrac{1}{2}\tau\hat{l}^2 + \kappa[\cos(\theta) + \varepsilon\sin(\theta)]\delta_p(t)\ ,\\ H_{\downarrow\downarrow} &= \langle\downarrow|\ H\ |\downarrow\rangle\\ &= \tfrac{1}{2}\tau\hat{l}^2 + \kappa[\cos(\theta) - \varepsilon\sin(\theta)]\delta_p(t)\ ,\\ H_{\updownarrow} &= \langle\downarrow|\ H\ |\uparrow\rangle = \tfrac{1}{2}\kappa\mu\sin(2\theta)\delta_p(t)\ . \end{aligned} \tag{4.15}$$

Then,

$$\begin{aligned} i\dot{\psi}^{\uparrow} &= H_{\uparrow\uparrow}\psi^{\uparrow} + H_{\updownarrow}\psi^{\downarrow}\ ,\\ i\dot{\psi}^{\downarrow} &= H_{\downarrow\downarrow}\psi^{\downarrow} + H_{\updownarrow}\psi^{\uparrow}\ . \end{aligned} \tag{4.16}$$

Defining $\alpha = \sqrt{2}\,A$, $\beta = \sqrt{2}\,B$, $\gamma = \sqrt{2}\,C$, $\eta = \sqrt{2}\,D$, the set (4.16) is equivalent with

$$\begin{aligned} \dot{\alpha} &= H_{\uparrow\uparrow}\beta + H_{\updownarrow}\eta\ ,\quad \dot{\beta} = -H_{\uparrow\uparrow}\alpha - H_{\updownarrow}\gamma\ ,\\ \dot{\gamma} &= H_{\downarrow\downarrow}\eta + H_{\updownarrow}\beta\ ,\quad \dot{\eta} = -H_{\downarrow\downarrow}\gamma - H_{\updownarrow}\alpha\ . \end{aligned} \tag{4.17}$$

Interpreting α and γ as generalized positions and β, η as generalized momenta, the set of equations (4.17) may be considered as classical equations derived from the Hamiltonian

$$H_{\rm cl} = \tfrac{1}{2}H_{\uparrow\uparrow}(\alpha^2+\beta^2) + \tfrac{1}{2}H_{\downarrow\downarrow}(\gamma^2+\eta^2) + H_{\updownarrow}(\beta\eta+\alpha\gamma) \tag{4.18}$$

via the canonical equations

$$\dot{\alpha} = \frac{\partial H_{\rm cl}}{\partial\beta},\quad \dot{\beta} = -\frac{\partial H_{\rm cl}}{\partial\alpha},\quad \dot{\gamma} = \frac{\partial H_{\rm cl}}{\partial\eta},\quad \dot{\eta} = -\frac{\partial H_{\rm cl}}{\partial\gamma}\ . \tag{4.19}$$

At this point we interpret $H_{\rm cl}$ as the classical version of (2.1) and therefore

$$\dot{\theta} = \frac{\partial H_{\rm cl}}{\partial l} = \tau l\ , \tag{4.20}$$

$$\begin{aligned} \dot{l} = -\frac{\partial H_{\rm cl}}{\partial\theta} &= \kappa\{\sin(\theta) - \tfrac{1}{2}\varepsilon[(\alpha^2+\beta^2)\\ &\quad -(\gamma^2+\eta^2)]\cos(\theta) - \mu(\beta\eta+\alpha\gamma)\cos(2\theta)\}\delta_p(t). \end{aligned} \tag{4.21}$$

Identifying $\alpha \equiv \sqrt{2}\,\Re\phi^{\uparrow}$, $\beta \equiv \sqrt{2}\,\Im\phi^{\uparrow}$, $\gamma \equiv \sqrt{2}\Re\phi^{\downarrow}$, $\eta \equiv \sqrt{2}\Im\phi^{\downarrow}$, it is easily seen that (4.10), (4.11), and (4.12) are equivalent (or even identical) to (4.20), (4.21), and (4.17), respectively. Therefore, both the mean-field and the Hamiltonian approach yield the same equations of motion for l and θ. In the next section, the equations of motion (4.12) [(4.17), respectively] will be solved in the form of a mapping.

C. The mapping equations for the mean-field model

Deriving a mapping for the mean-field equations (4.10)–(4.12) is not as simple as in the case of the standard kicked rotor. The reason is that the amplitudes $\phi^{\uparrow}$ and $\phi^{\downarrow}$ are discontinuous at a kick. But since their values at the kick are needed in (4.11) it is not immediately clear what this value should be. In order to resolve this problem, it is best to use a square integrable approximation of the δ function with finite width τ and perform the limit $\tau \to 0$ after (4.11) and (4.12) are integrated for finite τ. We choose

$$\delta(t) \sim \begin{cases} 1/\tau & \text{for } 0 \le t \le \tau\\ 0 & \text{otherwise}\ . \end{cases} \tag{4.22}$$

Denoting by ϕ_m, θ_m, the values of ϕ and θ immediately before kick number m, we have for $0 \le t \le \tau$

$$\begin{aligned} \phi(t) \;=\; \exp\Bigg(&-i\frac{\kappa t}{\tau}[\varepsilon\sin(\theta_m)\sigma_z\\ &+ \tfrac{1}{2}\mu\sin(2\theta_m)\sigma_x]\Bigg)\ \phi_m\ . \end{aligned} \tag{4.23}$$

This expression can be used to integrate l in the interval $0 \le t \le \tau$ when replacing $\delta_p(t)$ in (4.11) by (4.22). The calculations are straightforward and will not be reported here. Denoting by l_{m+1}, θ_{m+1}, ϕ_{m+1} the values of the variables immediately before kick number $m+1$ we obtain the following mapping for l in the limit $\tau \to 0$:

$$l_{m+1} = l_m + \kappa \sin(\theta_m) - \kappa\varepsilon \cos(\theta_m) A_m - 2\kappa\mu \cos(\theta_m) B_m \ ,$$

$$A_m = [|\phi_m^{\uparrow}|^2 - |\phi_m^{\downarrow}|^2] \left[I_c - I_s \frac{\mu^2}{s^2} \sin^2(\theta_m) + I_s \frac{\varepsilon^2}{s^2} \sin^2(\theta_m) \right] + 2 I_{\rm SC} \frac{\mu}{s} \sin(2\theta_m) \Im[{\phi_m^{\uparrow}}^* \phi_m^{\downarrow}]$$
$$+ 4 I_s \frac{\varepsilon\mu}{s^2} \sin(\theta_m) \sin(2\theta_m) \Re[{\phi_m^{\uparrow}}^* \phi_m^{\downarrow}] \ , \qquad (4.24)$$

$$B_m = 2 \left[I_c + I_s \frac{\mu^2}{s^2} \sin^2(2\theta_m) - I_s \frac{\varepsilon^2}{s^2} \sin^2(\theta_m) \right] \Re[{\phi_m^{\uparrow}}^* \phi_m^{\downarrow}] - 2 I_{\rm SC} \frac{\varepsilon}{s} \sin(\theta_m) \Im[{\phi_m^{\uparrow}}^* \phi_m^{\downarrow}]$$
$$+ 2 I_s \frac{\varepsilon\mu}{s^2} \sin(\theta_m) \sin(2\theta_m) [|\phi_m^{\uparrow}|^2 - |\phi_m^{\downarrow}|^2] \ ,$$

where

$$I_c = \frac{1}{2} + \frac{1}{4\kappa s} \sin(2\kappa s) \ ,$$
$$I_{\rm SC} = \frac{1}{\kappa s} [1 - \cos(2\kappa s)] \ , \qquad (4.25)$$
$$I_s = \frac{1}{2} - \frac{1}{4\kappa s} \sin(2\kappa s) \ ,$$

and

$$s = \sqrt{\varepsilon^2 \sin^2(\theta) + \tfrac{1}{4}\mu^2 \sin^2(2\theta)} \ . \qquad (4.26)$$

Since l is constant between kicks we get immediately from (4.10)

$$\theta_{m+1} = \theta_m + \tau l_{m+1} \ . \qquad (4.27)$$

For $t = \tau$, (4.23) yields

$$\phi_{m+1}^{\uparrow} = \left(\cos(\kappa s) - i \frac{\varepsilon}{s} \sin(\kappa s) \sin(\theta_m) \right) \phi_m^{\uparrow} - i \frac{\mu}{s} \sin(\kappa s) \sin(2\theta_m) \, \phi_m^{\downarrow} \ ,$$
$$\phi_{m+1}^{\downarrow} = \left(\cos(\kappa s) + i \frac{\varepsilon}{s} \sin(\kappa s) \sin(\theta_m) \right) \phi_m^{\downarrow} - i \frac{\mu}{s} \sin(\kappa s) \sin(2\theta_m) \, \phi_m^{\uparrow} \ . \qquad (4.28)$$

The mapping (4.24)–(4.28) can be used to calculate staying probabilities and the classical diffusion constants for the symplectic kicked rotor (2.1). The dots in Fig. 8 labeled "mean field" show $P_s(n)$ for $\tau = \hat{\tau}$, $\kappa = \hat{k}$, $\varepsilon = 0.3$, and $\mu = 0.8$ calculated with the mapping (4.24)–(4.28). We used $l_0 = 0$, $\phi_0^{\uparrow} = 1$, $\phi_0^{\downarrow} = 0$, and 10^5 initial θ values equidistributed in $[0, 2\pi]$. Furthermore, in order to improve the statistics, the staying probability $P_s(n)$ was time averaged over five kicks. The full line in Fig. 8 is a fit to the mean-field $P_s(n)$ data. It decays as $1/\sqrt{n}$ which is the correct behavior for a diffusion process. In fact, for a classical diffusion process we expect [22]

$$P_s(n) = \frac{1}{\sqrt{2\pi D n}} \ . \qquad (4.29)$$

On the basis of (4.29), a diffusion constant $D \approx 10^3$ can be extracted from the straight line fit to the data points in Fig. 8. This figure also shows that the diffusion in the mean-field model never stops. This means that due to the classical approximation in $\hat{l}$ and $\hat{\theta}$ (4.24)–(4.28) does not show any localization effects.

Clearly the mapping (4.24)–(4.28) is very complicated and analytical approximations to the diffusion constant are desirable. In the next section we will discuss an alternative approach which yields an analytical estimate of the classical diffusion constant.

D. Quantum energy mapping

An approximation to the classical diffusion constant can be obtained from the energy mapping of the generalized kicked rotor (2.1). The energy of the rotor immediately before kick number n is defined as

$$E_n = \langle \psi_n \mid \hat{l}^2 \mid \psi_n \rangle = \langle \psi_0 \mid {U^{\dagger}}^n \hat{l}^2 U^n \mid \psi_0 \rangle \ , \qquad (4.30)$$

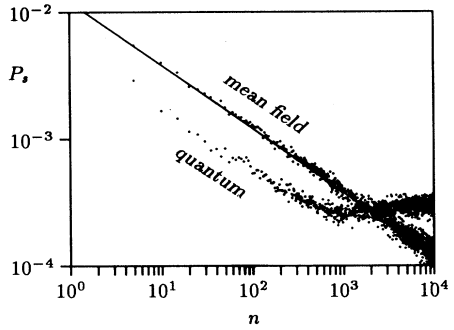

FIG. 8. Total staying probabilities (sum over spin-up and spin-down components) of the symplectic kicked rotor ($\beta = 4$) for the same parameters as in Fig. 7 for the mean-field and quantum approaches. In both cases the initial spin state was $|\uparrow\rangle$. Full line: $1/\sqrt{n}$ fit to the mean-field staying probability.

where U is the complete rotor propagator over one kick (the one-cycle operator) and ψ_0 is the starting state. To find the energy mapping we use

$$E_{n+1} = \langle \psi_{n+1} \mid \hat{l}^2 \mid \psi_{n+1} \rangle = \langle \psi_n \mid U^\dagger \hat{l}^2 U \mid \psi_n \rangle \quad . \tag{4.31}$$

The complete one-cycle propagator factorizes into

$$U = \exp\{-i\tfrac{1}{2}\tau \hat{l}^2\} V \ , \tag{4.32}$$

with

$$V = e^{-i\kappa\cos(\theta)} e^{-i\kappa s(\mathbf{v}\cdot\boldsymbol{\sigma})} \quad . \tag{4.33}$$

Here

$$\mathbf{v} = \frac{1}{s} \begin{pmatrix} \frac{1}{2}\mu \sin(2\theta) \\ 0 \\ \varepsilon \sin(\theta) \end{pmatrix} \tag{4.34}$$

and s was defined in (4.26). Using the factorization (4.32), we arrive at

$$E_{n+1} = \langle \psi_n \mid U^\dagger \hat{l}^2 U \mid \psi_n \rangle = \langle \psi_n \mid (\hat{l}V)^\dagger \hat{l} V \mid \psi_n \rangle \quad . \tag{4.35}$$

Using the identity $\hat{l}V = [\hat{l}, V] + V\hat{l}$ with $\hat{l} = -i\frac{\partial}{\partial\theta}$ we get

$$\hat{l}V = V[\hat{l} + \kappa\sin(\theta)] + e^{-i\kappa\cos(\theta)}[\hat{l}, e^{-i\kappa s(\mathbf{v}\cdot\boldsymbol{\sigma})}] \quad . \tag{4.36}$$

The commutator in (4.36) is given by

$$-\kappa s'(\mathbf{v}\cdot\boldsymbol{\sigma}) e^{-i\kappa s(\mathbf{v}\cdot\boldsymbol{\sigma})} - (\mathbf{v}'\cdot\boldsymbol{\sigma})\sin(\kappa s) \ , \tag{4.37}$$

where the primes denote differentiation with respect to θ. With this expression (4.36) becomes

$$\begin{aligned} \hat{l}V = V[\hat{l} + \kappa\sin(\theta) - \kappa s'(\mathbf{v}\cdot\boldsymbol{\sigma})] \\ -e^{-i\kappa\cos(\theta)} (\mathbf{v}'\cdot\boldsymbol{\sigma})\sin(\kappa s). \end{aligned} \tag{4.38}$$

Multiplying (4.38) with its Hermitian conjugate we obtain a result which consists of spin independent and spin dependent terms, respectively:

$$(\hat{l}V)^\dagger \hat{l}V = F_0 - F_\sigma. \tag{4.39}$$

Here,

$$F_0 = [\hat{l} + \kappa\sin(\theta)]^2 + \kappa^2 (s')^2 + (\mathbf{v}')^2 \sin^2(\kappa s) \tag{4.40}$$

and

$$\begin{aligned} F_\sigma = \kappa[\hat{l}s'(\mathbf{v}\cdot\boldsymbol{\sigma}) + s'(\mathbf{v}\cdot\boldsymbol{\sigma})\hat{l}] + 2\kappa^2 s'(\mathbf{v}\cdot\boldsymbol{\sigma})\sin(\theta) + 2\kappa\sin(\theta)\sin(\kappa s)[(\mathbf{v}'\cdot\boldsymbol{\sigma})\cos(\kappa s) - (\mathbf{v}\cdot\boldsymbol{\sigma})\sin(\kappa s)] \\ +[\hat{l}e^{i\kappa s(\mathbf{v}\cdot\boldsymbol{\sigma})}(\mathbf{v}'\cdot\boldsymbol{\sigma})\sin(\kappa s) + (\mathbf{v}'\cdot\boldsymbol{\sigma})e^{-i\kappa s(\mathbf{v}\cdot\boldsymbol{\sigma})}\sin(\kappa s)\hat{l}] \quad . \end{aligned} \tag{4.41}$$

We note that the term in square brackets in (4.40) is exactly the one for the standard kicked rotor.

$$\begin{aligned} [\hat{l} + \kappa\sin(\theta)]^2 = \hat{l}^2 + \tfrac{1}{2}\kappa^2 - \tfrac{1}{2}\kappa^2\cos(2\theta) \\ +\kappa[\hat{l}\sin(\theta) + \sin(\theta)\hat{l}] \quad . \end{aligned} \tag{4.42}$$

Neglecting the spin dependent contribution F_σ, which is expected to be small, we obtain the energy mapping

$$\begin{aligned} E_{n+1} = \langle \psi_n \mid [\hat{l} + \kappa\sin(\theta)]^2 + \kappa^2 (s')^2 \\ +(\mathbf{v}')^2 \sin^2(\kappa s) \mid \psi_n \rangle \quad . \end{aligned} \tag{4.43}$$

The right-hand side of (4.43) can be evaluated approximately by assuming that $\langle \theta \mid \psi_n \rangle$ is equidistributed in θ. Using $E_n = \langle \psi_n \mid \hat{l}^2 \mid \psi_n \rangle$, $\langle \psi_n \mid \cos(2\theta) \mid \psi_n \rangle \approx 0$, $\langle \psi_n \mid \hat{l}\sin(\theta) + \sin(\theta)\hat{l} \mid \psi_n \rangle \approx 0$ we obtain

$$E_{n+1} = E_n + D(\kappa; \varepsilon, \mu) \ , \tag{4.44}$$

where

$$D(\kappa; \varepsilon, \mu) = \tfrac{1}{2}\kappa^2 + \Delta D(\kappa; \varepsilon, \mu) \ , \tag{4.45}$$

with

$$\Delta D(\kappa; \varepsilon, \mu) = \frac{1}{2\pi} \int_0^{2\pi} d\theta [\kappa^2 (s')^2 + (\mathbf{v}')^2 \sin^2(\kappa s)] \quad . \tag{4.46}$$

The term $\kappa^2/2$ corresponds to the lowest-order diffusion constant of the standard kicked rotor. To this the spin dependent parts in the Hamiltonian (2.2) contribute approximately ΔD given in (4.46).

It can be checked numerically that for the cases of interest here the second term in (4.46) is on the order of 1, while the first term is of order $\kappa^2 \gg 1$. Therefore (4.46) can be approximated by

$$\Delta D(\kappa; \varepsilon, \mu) = \frac{\kappa^2}{2\pi} \int_0^{2\pi} (s')^2 d\theta \quad . \tag{4.47}$$

The integral in (4.47) can be evaluated analytically so that (4.45) finally reads

$$D(\kappa; \varepsilon, \mu) = \frac{\kappa^2}{2}[1 + 2I(\varepsilon, \mu)] \ , \tag{4.48}$$

with

$$I(\varepsilon, \mu) = \frac{(\varepsilon^2 + \mu^2)^2}{\mu^2} \left[1 - \frac{\varepsilon}{\sqrt{\varepsilon^2 + \mu^2}} \right] - \tfrac{1}{2}\mu^2 \quad . \tag{4.49}$$

Figure 9 shows the ratio $R(p, q) = D/(k^2/2)$ where D is the diffusion constant defined in (4.48). Note that R does not depend on k. It is a function of p and q only. This can easily be shown using the transformation formulas (2.3) and (2.4). Figure 9 gives a good impression of the behavior of $R(p, q)$. It can be checked immediately that (4.48)

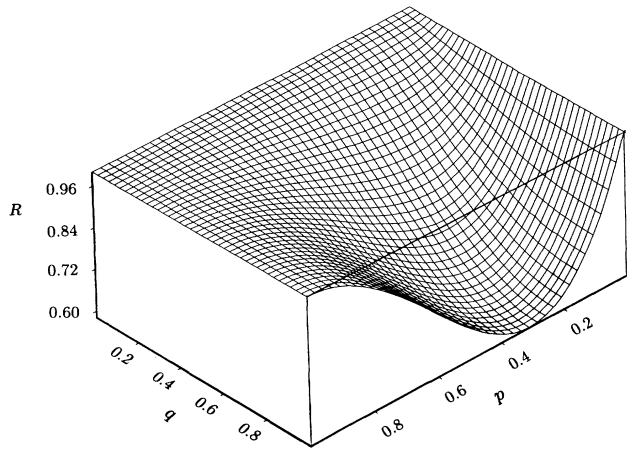

FIG. 9. Normalized analytical diffusion constant $R(p,q)$ of the symplectic kicked rotor as a function of the two symmetry-breaking parameters p and q.

yields the correct zero-order diffusion constant $D = k^2/2$ in the limits $\varepsilon = 0$, μ arbitrary and $\mu = 0$, ε arbitrary.

If the time evolution of the symplectic rotor wave function $|\psi\rangle$ were purely diffusive and governed by the diffusion constant D in (4.48), we would expect that the staying probability for the symplectic rotor decays according to (4.29). For the parameters used in Fig. 8, the analytical prediction for the diffusion constant on the basis of (4.48) is $D = 1115$. This value for D is in excellent agreement with the diffusion constant $D \approx 10^3$ extracted from the straight line fit to the mean-field data (full line in Fig. 8).

E. Quantum calculations

Solving the time dependent Schrödinger equation for the nonresonant symplectic kicked rotor does not pose any difficulties. We used the standard fast Fourier method adapted to the present case to propagate the rotor wave function. As a first application we calculated numerically the exact quantum staying probability for the symplectic rotor for the same parameter set as was used in Fig. 8 to calculate the mean-field staying probability. Averaging the staying probability over a large set of l_0 values as described in (3.11), we obtain the result marked "quantum" displayed in Fig. 8. Just as in the case of the mean-field model, the quantum staying probabilities were locally time averaged over five kicks for a better overall statistics. The quantum staying probability is seen to be a factor of 2 lower than both the classical mean-field staying probability and the staying probability calculated on the basis of (4.29) with D calculated from (4.48). This is weak antilocalization.

The quantum staying probability displayed in Fig. 8 can also be used to verify the scaling law (3.25) for the symplectic ($\beta = 4$) case. From the asymptotic value of the staying probability we extracted the participation ratio ξ and defined the scaled time $x = 4n/\xi$. Plotting $\xi P_s(n)$ versus x we obtain the bullets shown in Fig. 7. We see that the f function for the CSE case (bullets) is very close to the corresponding f functions for the COE and the CUE cases. There are, however, statistically significant oscillations in the f function of the CSE case which deserve further study. Thus we established that apart from the apparent oscillations the scaling relation (3.25) also holds for $\beta = 4$.

In order to prove (1.1) for the symplectic kicked rotor as an example of a dynamically localizing system, we calculated the proportionality constant c which relates the participation ratio to the diffusion constant according to

$$\xi = cD \quad . \tag{4.50}$$

In order to evaluate c we calculated the diffusion constant D quantum mechanically according to

$$D^{(qm)} = \tfrac{1}{200} \sum_{n=1}^{200} |\langle \psi_n | \hat{l}^2 | \psi_n \rangle|^2 \; / \; n \quad . \tag{4.51}$$

The participation ratio is inversely proportional to P_a, the asymptotic probability to stay in the initial state $|\psi_0\rangle$:

$$P_a = \lim_{N\to\infty} \frac{1}{N - n^*} \sum_{n=n^*}^{N} |\langle \psi_n | \psi_0 \rangle|^2 \quad . \tag{4.52}$$

This way we get

$$c = \frac{1}{D^{(qm)} P_a} \quad . \tag{4.53}$$

Figure 10 shows the normalized proportionality constant $\hat{c} = c/c(\beta = 1)$ as a function of x for $y = 0$ and $\tau = \hat{\tau}$, $k = \hat{k}$. As x sweeps from -10 to 5, $\hat{c}$ shows jumps and plateaus. The plateaus coincide exactly with the CUE, CSE, and COE phases of H, respectively. The jumps occur in the transition regions between well established symmetry classes [compare Fig. 2(a)]. Figure 10 convincingly proves the relation (1.1) for a system with dynamical localization.

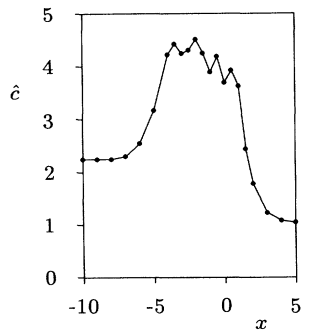

FIG. 10. Normalized proportionality constant $\hat{c} = c(\beta)/c(\beta = 1)$ for $y = 0$ ($q = \frac{1}{2}$) as a function of x. The function changes sharply by universal factors at the boundaries between universality classes (compare Fig. 2).

V. DISCUSSION, SUMMARY, AND CONCLUSIONS

The dependence of the localization length on the universality class was derived in the previous sections indirectly by computing staying probabilities. The staying probabilities were normalized to the quantum diffusion constant $D^{(qm)}$ in the diffusive regime. With the help of detailed calculations we checked that the results summarized in Fig. 10 do not change qualitatively if they are normalized to the diffusion constant calculated with the mean-field approach. Even using the analytical diffusion constant does not change this result.

A more important question is whether the dependence of the localization length on the universality class can be demonstrated directly. At this point we can give a partial answer which applies to the COE $\rightarrow$ CUE transition. We focused on the case $K = 5$, $\tau = \hat{\tau}$, $k = 5/\hat{\tau}$, $p = 0$ and computed quasienergy states by a direct diagonalization of the one-cycle operator for various choices of q. Our basis size was $B = 1024$. For every given q value we chose ten l_0 values given by $l_0 = 5000, 10\,000, ..., 50\,000$. The quasienergy states obtained were evaluated in the following two different ways.

(i) We picked 21 states around each of the l_0 values and calculated their participation ratio $\xi(q)$. Averaging over the resulting 210 ξ values we obtained a global participation ratio denoted by $\bar{\xi}(q)$.

Figure 11 shows $\bar{R} = D(q=0)\bar{\xi}(q)/D(q)\bar{\xi}(q=0)$ for a range of q values. Here, D is the classical diffusion constant which properly normalizes the quantum participation ratios. The classical diffusion constant was obtained numerically by a Monte Carlo calculation with 10^5 trajectories.

The transition from $\bar{R} = 1$ to $\bar{R} \approx 2$ is clearly visible in Fig. 11. Thus, using an alternative and independent method of determining ξ, we have shown that the factor-of-2 increase in the localization length is "real" and not an artifact of the particular method used to evaluate the participation ratio ξ.

(ii) A direct demonstration of the influence of symmetry on the localization length of quasienergy states can be obtained by looking directly at the quasienergy states themselves. The problem here is that the localization length of quasienergy states fluctuates dramatically [8]. Therefore assigning a localization length for given control parameters k, τ, p, q makes sense only if we average over the localization lengths of many quasienergy states. We obtained averaged quasienergy states in the following way. For every one of the ten l_0 values defined above, we chose 20 quasienergy states with the largest overlap with l_0. This procedure ensures that the corresponding quasienergy states are well represented within the finite basis. This way we obtained 200 quasienergy states $|\alpha_j\rangle$, $j = 1, ..., 200$. For every one of the 200 states we calculated its l average, $\bar{l}_j$. The absolute square of the averaged quasienergy state $\langle m|\bar{\alpha}\rangle$, $m = ..., -2, -1, 0, 1, 2, ...$, is now defined according to

$$|\langle m|\bar{\alpha}\rangle|^2 = \exp\left(\frac{1}{200}\sum_{j=1}^{200} \ln[|\langle m + \bar{l}_j|\alpha_j\rangle|^2]\right). \quad (5.1)$$

Figure 12 shows the resulting two averaged quasienergy states for $q = 0$ and 0.1. The change in localization length is clearly visible. This is the most direct test of the influence of symmetry on the localization length. We note that the definition (5.1) can be generalized and that the concept of the average quasienergy state can be used generally to overcome the fluctuation problem [8] of the quasienergy states.

Due to basis size problems we were not yet able to check the factor-of-4 increase in the localization length in the CSE case by direct diagonalization of the one-cycle propagator. We feel that this check is important. It is currently under active investigation.

In summary, we have shown that the localization length of the symplectic kicked rotor depends smoothly on the strength of the symmetry-breaking interactions. Normalizing to the diffusion properties of the classical system we established that the localization length of the kicked rotor reflects the universality class according to (1.1) above. In the CUE limit we derived explicit semiclassical formulas which qualitatively reproduce the transition of the localization length between the symmetric and the symmetry-broken cases. It was shown that the critical field strength needed to break the symmetry can be evaluated by requiring that the rms of the action due to the symmetry-breaking force acting during the local-

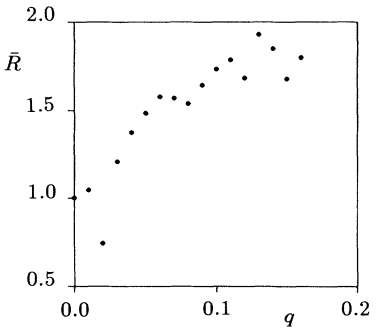

FIG. 11. Normalized participation ratio $\bar{R}(q)$ for a range of q values in the transition region COE $\rightarrow$ CUE.

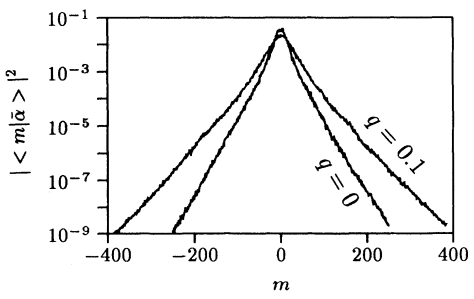

FIG. 12. Ensemble averaged quasienergy states for $p = 0$, $q = 0$ (COE case) and $p = 0$, $q = 0.1$ (CUE case).

ization time $n^* \approx \xi$ is of order $\hbar$ (=1). This is an intuitively clear requirement and it was proposed in a different context by Sivan and Imry [37]. Finally, the scaling relation (3.25) first proposed in Ref. [22] for the symmetric kicked rotor was generalized to include all three universality classes.

As a last point we would like to emphasize that we studied here a quantum system which is analogous to a quasi-one-dimensional disordered system. It is not clear at all whether similar results apply to higher-dimensional systems. This is an important open problem which calls for further research.

ACKNOWLEDGMENTS

The extensive computations whose results are reported in this paper were only possible with the help of a generous grant to R.B. from the University of Delaware Research Foundation (UDRF). R.B. is also grateful for financial support from the Deutsche Forschungsgemeinschaft (DFG). U.S. is grateful for a Minerva grant. We gratefully acknowledge constructive discussions with S. Fishman, F. M. Izrailev, D. L. Shepelyansky, R. Graham, and Y. Imry.

[1] C. E. Porter, *Statistical Theory of Spectra: Fluctuations* (Academic, New York, 1965).
[2] P. W. Anderson, Phys. Rev. **109**, 1492 (1958).
[3] G. Casati, B. V. Chirikov, F. M. Izrailev, and J. Ford, in *Stochastic Behavior in Classical and Quantum Hamiltonian Systems*, edited by G. Casati and J. Ford, Lecture Notes in Physics Vol. 93 (Springer, Berlin, 1979), p. 334.
[4] B. V. Chirikov, F. M. Izrailev, and D. L. Shepelyansky, Sov. Sci. Rev. Sect. C **2**, 209 (1981).
[5] S. Fishman, D. R. Grempel, and R. E. Prange, Phys. Rev. Lett. **49**, 509 (1982).
[6] D. L. Shepelyansky, Phys. Rev. Lett. **56**, 677 (1986).
[7] R. Blümel, S. Fishman, M. Griniasti, and U. Smilansky, in *Quantum Chaos and Statistical Nuclear Physics*, edited by T. H. Seligman and H. Nishioka, Lecture Notes in Physics Vol. 263 (Springer, Berlin, 1986).
[8] F. M. Izrailev, Phys. Rep. **196**, 299 (1990).
[9] R. Blümel and U. Smilansky, Phys. Rev. Lett. **52**, 137 (1984).
[10] R. Blümel and U. Smilansky, Phys. Rev. A **30**, 1040 (1984).
[11] G. Casati, B. V. Chirikov, I. Guarneri, and D. L. Shepelyansky, Phys. Rep. **154**, 77 (1987).
[12] R. Blümel, A. Buchleitner, R. Graham, L. Sirko, U. Smilansky, and H. Walther, Phys. Rev. A **44**, 4521 (1991).
[13] K. B. Efetov and A. I. Larkin, Zh. Eksp. Teor. Fiz. **85**, 764 (1983) [Sov. Phys. JETP **58**, 444 (1983)].
[14] J.-L. Pichard, M. Sanquer, K. Slevin, and P. Debray, Phys. Rev. Lett. **65**, 1812 (1990).
[15] R. Scharf, J. Phys. A **22**, 4223 (1989).
[16] F. J. Dyson, J. Math. Phys. **3**, 140 (1962).
[17] M. L. Mehta, *Random Matrices* (Academic, Boston, 1991).
[18] F. Haake, *Quantum Signatures of Chaos* (Springer-Verlag, Berlin, 1991).
[19] A. B. Rechester and R. B. White, Phys. Rev. Lett. **44**, 1586 (1980).
[20] A. B. Rechester, M. N. Rosenbluth, and R. B. White, Phys. Rev. A **23**, 2664 (1981).
[21] R. Blümel and U. Smilansky, Phys. Rev. Lett. **69**, 217 (1992).
[22] T. Dittrich and U. Smilansky, Nonlinearity **4**, 59 (1991); **4**, 85 (1991).
[23] B. V. Chirikov, Phys. Rep. **52**, 263 (1979).
[24] D. R. Grempel, R. E. Prange, and S. Fishman, Phys. Rev. A **29**, 1639 (1984).
[25] M. Robnik and M. V. Berry, J. Phys. A **19**, 669 (1986).
[26] Ya. B. Zeldovich, Zh. Eksp. Teor. Fiz. **51**, 1492 (1967) [Sov. Phys. JETP **24**, 1006 (1967)].
[27] F. M. Izrailev, Phys. Rev. Lett. **56**, 541 (1986).
[28] M. Feingold, S. Fishman, D. R. Grempel, and R. E. Prange, Phys. Rev. B **31**, 6852 (1985).
[29] S. A. Molcanov, Commun. Math. Phys. **78**, 429 (1981).
[30] D. A. deWolf, IEEE Trans. Ant. Prop. **19**, 254 (1971).
[31] A. Golubenter, Zh. Eksp. Teor. Fiz. **86**, 47 (1984) [Sov. Phys. JETP **59**, 26 (1984)].
[32] E. Akkermans and R. Maynard, J. Phys. (Paris) **46**, L1045 (1985).
[33] S. John, Phys. Rev. Lett. **53**, 2169 (1984).
[34] S. John, Phys. Rev. Lett. **58**, 2486 (1987).
[35] P. W. Anderson, Philos. Mag. B **52**, 505 (1985).
[36] We are indebted to D. Shepelyansky for pointing this test out to us.
[37] U. Sivan and Y. Imry, Phys. Rev. B **35**, 6074 (1987).